Shellwise Mackay Transformation in Iron Nanoclusters

Georg Rollmann,[1] Markus E. Gruner,[1] Alfred Hucht,[1] Ralf Meyer,[1] Peter Entel,[1]
Murilo L. Tiago,[2] and James R. Chelikowsky[2,3]

[1]*Physics Department, University of Duisburg-Essen, 47048 Duisburg, Germany*
[2]*Center for Computational Materials, Institute for Computational Engineering and Sciences, University of Texas, Austin, Texas 78712, USA*
[3]*Departments of Physics and Chemical Engineering, University of Texas, Austin, Texas 78712, USA*

(Received 1 October 2006; published 24 August 2007)

Structure and magnetism of iron clusters with up to 641 atoms have been investigated by means of density functional theory calculations including full geometric optimizations. Body-centered cubic (bcc) isomers are found to be lowest in energy when the clusters contain more than about 100 atoms. In addition, another stable conformation has been identified for magic-number clusters, which lies well within the range of thermal energies as compared to the bcc isomers. Its structure is characterized by a close-packed particle core and an icosahedral surface, while intermediate shells are partially transformed along the Mackay path between icosahedral and cuboctahedral geometry. The gradual transformation results in a favorable bcc environment for the subsurface atoms. For Fe_{55}, the shellwise Mackay-transformed morphology is a promising candidate for the ground state.

DOI: 10.1103/PhysRevLett.99.083402 PACS numbers: 36.40.Mr, 31.15.Ew, 61.46.Bc, 61.46.Df

Transition-metal nanoclusters of the ferromagnetic elements in the late 3*d* series have raised much attention in the past, as their properties deviate considerably from bulk, e.g., by showing a significantly enhanced magnetic moment for sizes up to a few hundred atoms [1,2]. Furthermore, they act as partners for technologically relevant alloys as FePt and CoPt, which are currently discussed as storage media for ultra-high density magnetic recording [3]. Since the magnetic properties of the particles depend essentially on their geometric structures, a detailed knowledge of their morphologies and growth modes is of basic interest. For Ni and Co clusters containing up to 800 atoms, regularly spaced peaks in the mass spectra at certain magic cluster sizes have been interpreted as icosahedral growth patterns [4]. For iron, however, a competition of structures is suggested. Other experimental results confirm the stability of icosahedral isomers at least for small Fe clusters with a few dozens of atoms [5], whereas high resolution transmission electron microscopy of particles of 6 nm in diameter [6] rather suggest a body-centered cubic (bcc) lattice structure. For many systems [7,8], a crossover from icosahedral to cuboctahedral geometries is expected with decreasing surface to volume ratio. The surfaces of the icosahedra are comprised of 20 triangular (111) faces, but icosahedral structures are noncrystallographic and exhibit an intrinsic distortion. In contrast to that, cuboctahedral clusters have a perfect face-centered cubic (fcc) packing but also possess six (100) faces with a comparatively small coordination of the surface atoms.

Recently, the magnetism of Fe clusters with up to 400 atoms was studied in an extensive fixed-geometry *ab initio* investigation [9]. Within this work, we provide independently from experiment a systematic insight into the size dependence of structural properties of Fe clusters from first principles. This approach includes full geometric optimizations—which have considerable influence on the magnetic structure of non-bcc isomers—of selected geometries of Fe clusters containing up to 5 complete atomic shells. The calculations were performed on the IBM Blue Gene/L supercomputer at Forschungszentrum Jülich on up to 1024 processors simultaneously.

The number of atoms N in perfect icosahedra as well as fcc cuboctahedra with n complete atomic shells is given by the sequence $N = (10n^3 + 15n^2 + 11n + 3)/3$, which yields $N = 13, 55, 147, 309, 561$, etc. Clusters with bcc structure, which is the ground state of bulk iron, of equal number of atoms can be obtained by applying a Bain transformation [10] to the cuboctahedra. A transformation path between perfect icosahedra and cuboctahedra was proposed by Mackay [11]. As shown in Fig. 1, pairs of adjacent triangular faces of the icosahedron (ICO) are transformed into square faces of the cuboctahedron

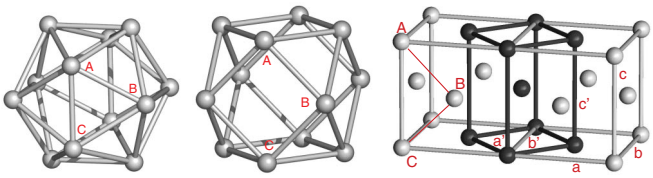

FIG. 1 (color). Left and center: Icosahedron and cuboctahedron. During the Mackay transformation, the bond $\overline{AC}$ (left) stretches and the two adjacent triangles turn into the same plane. Right: Face-centered cubic lattice with inscribed body-centered tetragonal Bain cell. The letters a, b, c represent the lattice vectors of the fcc lattice, whereas the primed letters refer to the bct structure. The Bain transformation is controlled by variation of c with respect to a and b. The capital letters refer to the same atomic sites in each structure.

(CUBO). The transformation path can be parameterized by the squared ratio of the stretched ($\overline{AC}$) to the unstretched ($\overline{AB}$) bonds, $s = (\overline{AC}/\overline{AB})^2$, with $s = 1$ for the ICO and $s = 2$ for the CUBO. Along the path, the system retains T_h symmetry, while at the endpoints it is I_h and O_h, respectively.

The calculations were performed in the framework of density functional theory (DFT) [12] with the Vienna Ab-initio Simulation Package (VASP) [13,14]. We used the generalized gradient approximation [15,16] in combination with the projector-augmented wave method [17] and a plane-wave basis set ($E_{\text{cut}} = 268$, 293, and 350 eV for $N \geq 147$, $N = 55$, and $N = 13$, respectively), requiring a sufficiently large supercell (up to $32 \times 32 \times 32$ Å^3 for $N = 561$) to separate the periodic images. The integration over the Brillouin zone was performed using the Γ point only. Cluster geometries were optimized with the conjugate gradient method until the energy difference between two consecutive iterations fell below 0.1 meV.

The energetic order of the optimized structures as a function of the cluster size is summarized in Fig. 2. The bcc clusters (Bain-transformed cuboctahedra) mark the energetic reference and are thus located on the abscissa. For the Fe_{13} cluster, we find in agreement with previous studies [19] a Jahn-Teller distorted ICO with a total magnetic moment of $44\mu_B$ and ferromagnetic alignment of the spins as ground state after full relaxation of the atoms

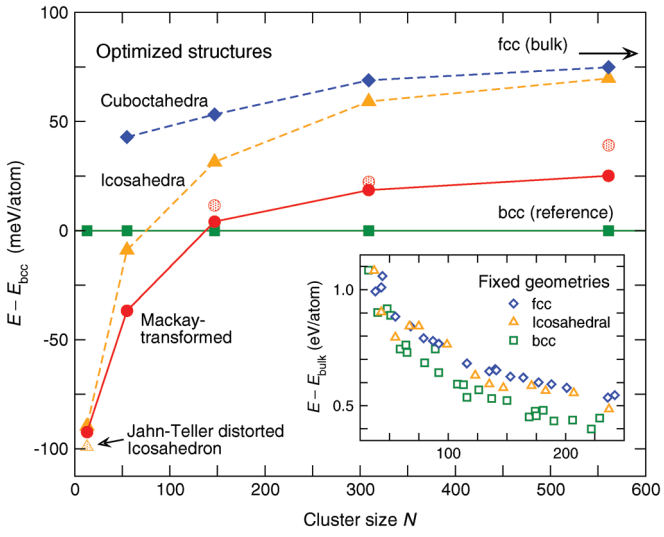

FIG. 2 (color). Total energy of optimized iron nanoclusters with complete atomic shells. The lines are only guides to the eye. Reference is the isomer with bcc structure which marks the ground state for bulk iron. The shellwise Mackay-transformed structure (circles) is preferred to the icosahedral (triangles) and cuboctahedral (diamonds) structures. Shaded circles mark Mackay-transformed clusters with different magnetic structures. For comparison, the energy of fcc bulk iron [18] is included. The inset shows the size dependence of the total energies of various geometries evaluated at the experimental bcc lattice constant. Reference is the energy of bulk bcc iron. Above 147 atoms, the bcc isomers are systematically lower in energy than all others.

without imposing any symmetry constraints. However, for $N = 55$ the energy of the ICO is close to the bcc reference and approaches with increasing size the energy of the cuboctahedra, which are higher in energy than the other morphologies throughout the entire size range and converge as expected against the bulk energy of fcc Fe. Fixed-geometry calculations of clusters with incomplete geometric shells using the PARSEC code as shown in the inset of Fig. 2 (for computational details, see [9]) underline the dominance of the bcc structures for larger sizes, since they are systematically lower in energy than cuboctahedra and icosahedra for $N \geq 59$. The energy differences, however, appear to be larger than for the optimized geometries, which can be related to the subtle interrelation between interatomic distance and magnetic structure in fcc Fe [20].

The circles in Fig. 2 refer to a previously unreported structure, which lies up to 45 meV/atom below the ICO at $N = 561$ and only 25 meV/atom above the bcc isomer. This structure, which we refer to as the shellwise Mackay-transformed (SMT) structure, evolves from icosahedra and cuboctahedra during geometric optimizations if stabilizing symmetry constraints are lifted and a small distortion along the Mackay path is imposed. It can be understood as a partial transformation of the shells along the Mackay path, with varying degree from the surface to the center. The shellwise resolved transformation parameter s as a function of the cluster size is depicted in Fig. 3. For larger clusters, the innermost shell turns into an almost perfect CUBO, while the outermost shell largely retains its icosahedral shape. Calculations of the harmonic vibrational frequencies of the three morphologies performed for $N = 55$ confirm the stability of the SMT structure as well as the instability of the other two against a Mackay-type distortion. The SMT Fe_{55} isomer is a special case, since its energy is also 37 meV/atom lower than the bcc reference, being a promising candidate for the ground state structure at this size. It possesses the same total magnetic moment of

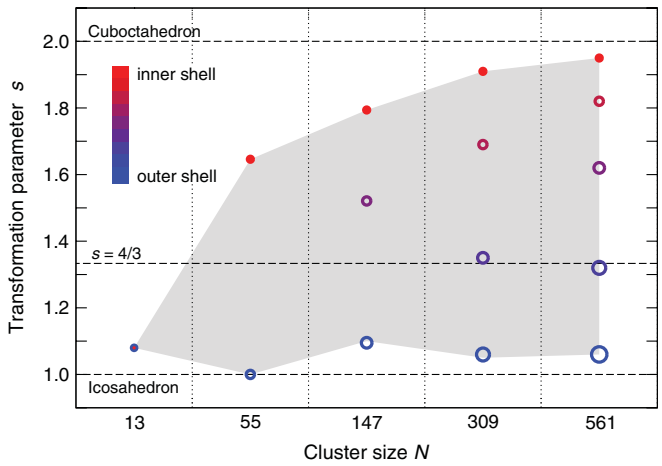

FIG. 3 (color). Degree of transformation in terms of s for each shell of the relaxed SMT structures. The colors indicate the relative shell position.

$150\mu_B$ as the undistorted ICO and CUBO (according to a ferromagnetic spin arrangement with a reversed central moment) but is energetically much more favorable (by 28 meV/atom and 80 meV/atom, respectively). Although the SMT is of T_h symmetry, its electronic ground state is nondegenerate, leaving no room for a Jahn-Teller distortion. The stability of the SMT geometry is retained when we take into account intra-atomic Coulomb repulsion of the Fe $3d$ electrons explicitly within the GGA + U method [21]. Furthermore, we noticed no significant dependence of the results on the choice of the generalized gradient approximation exchange-correlation functional.

In order to understand the mechanism behind this distortion a detailed structural analysis of the isomers was performed. We employed the common neighbor analysis [22,23], which is a standard tool for the interpretation of molecular dynamics simulations of structural transformations. The local environment of an atom is characterized by a set of signatures for neighboring atoms consisting of three indices defined by (i) the number of nearest neighbors both atoms have in common, (ii) the number of bonds between those neighbors, and (iii) the longest chain of bonds connecting them. In this way, fcc, bcc, and icosahedral geometries (and their surfaces) can be identified by a distinct set of signatures. The color coding in Fig. 4 compares the environment of the atoms in the SMT structure to their counterparts in fcc and bcc isomers within the first

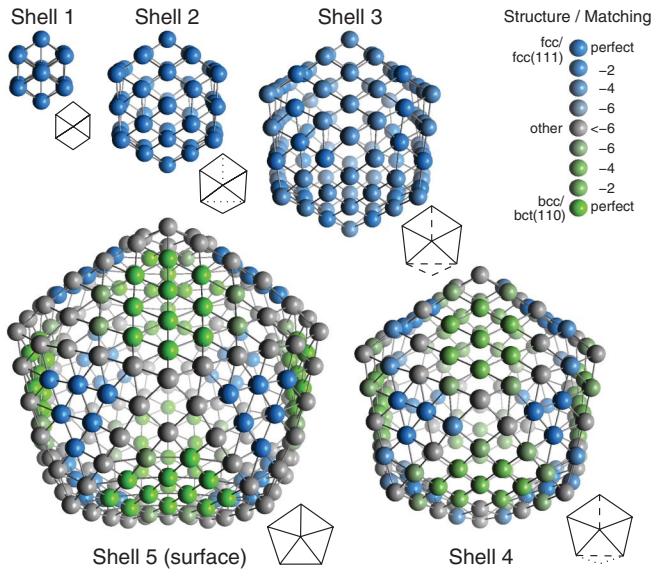

FIG. 4 (color). Shellwise Mackay-transformed Fe_{561}. For clarity, each shell is displayed separately. The small sketches depict the edges of the shell faces; broken lines represent edges in the process of disappearing/reappearing. The color coding refers to the result of the common neighbor analysis. Bright blue and green colors describe perfect matching of the signatures with corresponding atoms in perfect fcc or bcc clusters and on fcc(111) and bct(110) surfaces, respectively. The colors fade into gray (other structures) with increasing numbers of nonmatching signatures (in steps of 2).

(for bcc up to the second) neighbor shell. For the core, there is perfect matching with the CUBO, while large parts of the subsurface shell appear to have bcc-like coordination. This can also be seen in the pair correlation function. Figure 5 compares the coordination of the central atom and a subsurface edge atom with the distribution of neighbor distances of ideal fcc and bcc clusters, respectively. While the former fits almost perfectly, we find for the bcc case good agreement up to the third neighbor shell, after which deviations due to the increasing fcc character of the particle's core region as well as surface-shell distortions enter. There is a direct relationship between the transformation parameter s, which is close to $4/3$ in the subsurface shell, and the c/a ratio describing the transformation between fcc and bcc along the Bain path. The line $\overline{AC}$ in Fig. 1 corresponds to the c axis, while the perpendicular dropped from B onto $\overline{AC}$ corresponds to one half of the base diagonal of the body-centered tetragonal (bct) unit cell. Thus for a value of $\sqrt{3}/2$ for the ratio $\overline{AB}/\overline{AC}$ the ratio c'/a' becomes unity, which means perfect bcc. The fact that the two triangular faces of the ICO forming the (100) square of the CUBO are not in the same plane induces twinning stress along the common edge. For the edge center atoms, this is reduced by the considerable inward bending of the distorted edges (cf. inset of Fig. 5). For large parts of the surface shell, the agreement with the bcc isomer seems even better. However, this is partly due to a shortcoming of the common neighbor analysis, which does not distinguish properly between ideal and moderately tetragonal distorted bcc geometries. Following the considerations above, the green atoms rather describe a bct(110) surface with c'/a' close to $\sqrt{2/3}$.

The magnetic properties of the optimized iron clusters and their size dependence up to $N = 641$ are shown in Fig. 6. For comparison, the experimental results from

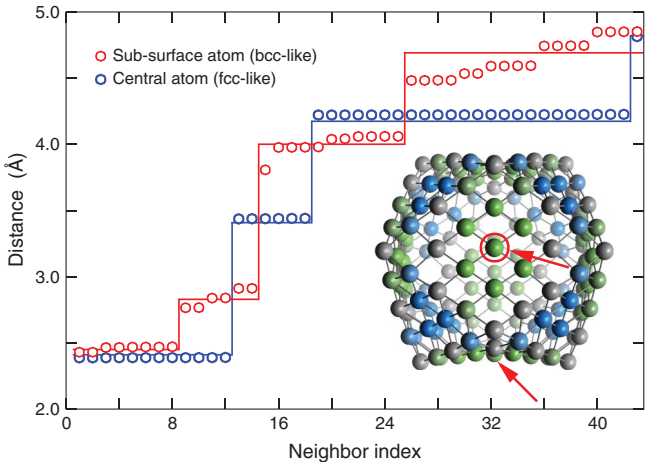

FIG. 5 (color). Distances between two atoms of SMT Fe_{561} and their neighbors. Blue: central atom. Red: edge center atom in the subsurface shell. The red arrows in the inset point to two of the six equivalent edge center positions in shell 4. The straight lines are the corresponding distances in ideal fcc and bcc structures.

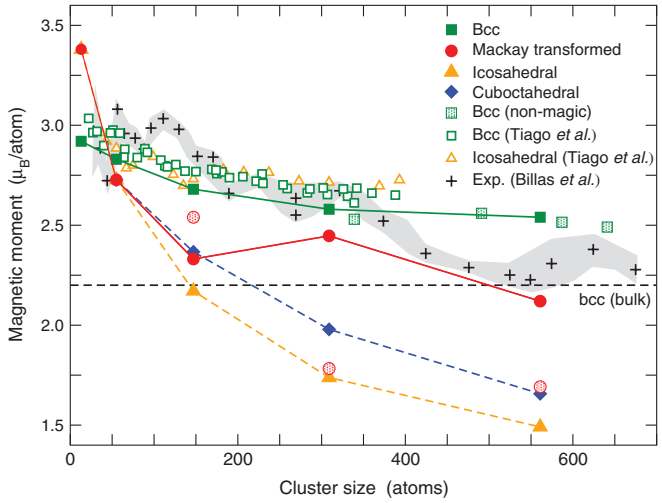

FIG. 6 (color). Magnetic moments of Fe clusters for different structures and cluster sizes (symbols as in Fig. 2). Lines are only guides to the eye. Optimized bcc clusters with sizes not corresponding to the closed shell ICO are denoted by shaded squares. Shaded circles refer to SMT isomers with magnetic configurations higher in energy (cf. Fig. 2). Open symbols denote the fixed-geometry values from [9]. The values are compared with experimental data (crosses) from [1,2]. The solid region marks the extension of the error bars. Bcc bulk data are taken from [18].

Stern-Gerlach experiments by Billas *et al.* [1,2] obtained at $T = 100$ K are included. One has to be aware that our DFT calculations do not take into account spin-orbit coupling and therefore only yield the spin moments, while the experimental data refer to the total moment. Spin-orbit coupling is expected to give an additional contribution especially for the smaller cluster sizes. The moments of the bcc isomers are in closest agreement with experiment for $N < 400$ and correspond well to the extensive DFT calculations by Tiago *et al.* [9], performed on nonrelaxed fixed-geometry Fe clusters. The small differences in magnitude are related to the compression of the core caused by the surface stress, which is taken care of by the structural optimizations. For the non-bcc isomers, the compression results in ferrimagnetic spin ordering, explaining the larger discrepancies to Ref. [9] in this case. For $N > 400$ the calculated moments exceed the experimental values significantly. A tentative extrapolation of the temperature dependent measurements published in [1] to $T = 0$ appears to close this gap. Nevertheless, for Fe_{561}, the lowest energy SMT isomer shows the best agreement with the experimental values at $T = 100$ K. The largely reduced energy difference to the bcc structure, which is in the range of thermal energies, suggests that under certain growth conditions SMT iron nanoclusters may be observed in experiments, giving a possible explanation for the pronounced minimum in the experimental magnetization curve.

As it was shown that SMT structures can be related to the affinity of iron toward bcc structures, these geometries may also be expected in particles made of other elements with bulk bcc structure as well as in composite (e.g., core-shell) systems, where one component favors a close-packed environment, the other a bcc-like environment. Such morphologies may be obtained after annealing the composites or by using appropriate wet chemical preparation methods. In this respect, first calculations have shown that empirical potentials, which were fitted to properties of the bulk phases of iron and nickel [24], are indeed capable of stabilizing SMT isomers in binary nanoparticles.

We thank the staff of the von Neumann Institute for Computing (NIC) in Jülich for their support and Dr. P. Vezolle of IBM for optimizing the VASP code for the Blue Gene/L system. This work was supported by the DFG through SFB 445. M. L. T. and J. R. C. acknowledge the support of the National Science Foundation under Grant No. DMR-0551195 and by the U.S. Department of Energy under DE-FG02-89ER45391 and DE-FG02-03ER15491.

[1] I. M. L. Billas *et al.*, Phys. Rev. Lett. **71**, 4067 (1993).
[2] I. M. L. Billas, J. A. Becker, and W. A. de Heer, Science **265**, 1682 (1994).
[3] S. Sun *et al.*, Science **287**, 1989 (2000).
[4] M. Pellarin *et al.*, Chem. Phys. Lett. **217**, 349 (1994).
[5] M. Sakurai *et al.*, J. Chem. Phys. **111**, 235 (1999).
[6] T. Vystavel *et al.*, Appl. Phys. Lett. **82**, 197 (2003).
[7] M. Baletto and R. Ferrando, Rev. Mod. Phys. **77**, 371 (2005).
[8] C. Barreteau *et al.*, Eur. Phys. J. D **11**, 395 (2000).
[9] M. Tiago *et al.*, Phys. Rev. Lett. **97**, 147201 (2006).
[10] E. C. Bain, Trans. Am. Inst. Min. Metall. Pet. Eng. **70**, 25 (1924).
[11] A. L. Mackay, Acta Crystallogr. **15**, 916 (1962).
[12] P. Hohenberg and W. Kohn, Phys. Rev. **136**, B864 (1964).
[13] G. Kresse and J. Furthmüller, Phys. Rev. B **54**, 11 169 (1996).
[14] G. Kresse and D. Joubert, Phys. Rev. B **59**, 1758 (1999).
[15] J. P. Perdew, K. Burke, and Y. Wang, Phys. Rev. B **54**, 16 533 (1996).
[16] J. P. Perdew, K. Burke, and M. Ernzerhof, Phys. Rev. Lett. **77**, 3865 (1996).
[17] P. E. Blöchl, Phys. Rev. B **50**, 17 953 (1994).
[18] H. C. Herper, E. Hoffmann, and P. Entel, Phys. Rev. B **60**, 3839 (1999).
[19] P. Bobadova-Parvanova *et al.*, Phys. Rev. B **66**, 195402 (2002).
[20] R. F. Sabiryanov, S. K. Bose, and O. N. Mryasov, Phys. Rev. B **51**, 8958 (1995).
[21] V. I. Anisimov, J. Zaanen, and O. K. Andersen, Phys. Rev. B **44**, 943 (1991).
[22] H. Jónsson and H. C. Andersen, Phys. Rev. Lett. **60**, 2295 (1988).
[23] D. Faken and H. Jónsson, Comput. Mater. Sci. **2**, 279 (1994).
[24] R. Meyer and P. Entel, Phys. Rev. B **57**, 5140 (1998).